INVESTIGATION OF SHOCK-INDUCED LCO OF A WING/STORE CONFIGURATION USING THE TRANSONIC SMALL DISTURBANCE METHOD

F. E. Eastep, N. S. Khot, P. S. Beran, J. V. Zweber and R. D. Snyder
Multidisciplinary Technologies Center, AFRL/VASD
Air Force Research Laboratory (AFRL), Air Vehicles Directorate
Wright-Patterson AFB, Ohio, 45433

Keywords: *Limit cycle oscillation, aeroelasticity*

Abstract

High performance fighter aircraft with specific external store configurations are susceptible to limit-cycle oscillation (LCO) in the transonic flight regime. LCO requires an accurate prediction of flow conditions which will initiate the oscillations. Although linear aerodynamics allows one to predict a critical flutter condition for a wing with various store configurations, LCO's typically occur at a speed somewhat below the linear predicted flutter speed. Here, transonic small disturbance (TSD) aerodynamic theory with interactive boundary layer is used to fully capture the features of LCO and predict its initiation. Although one of the simplest forms of nonlinear aerodynamics , TSD can identify the strength and location of weak shocks and is used here to predict the conditions for the initiation of LCO for a rectangular wing with a tip store placed in a transonic airstream. For the wing/store configuration investigated, limit cycle oscillations are obtained at speeds lower than those predicted for wing/store flutter with linear (no shocks) aerodynamics. LCO is shown to occur over a very limited range of Mach numbers and comparisons of LCO amplitudes are given for inviscid and viscous aerodynamics.

1 Nomenclature

α	angle of attack, degrees
c	chord, ft
cg, ea	center of gravity and elastic axis, ft from leading edge
C_L,	lift coefficient
M	Mach number
Re	Reynolds number
ρ	density, slugs/ft^3
t	time, nondimensional (based on free stream velocity and wing chord)
τ	thickness to chord ratio
U	velocity, ft/sec
ζ	structural damping coefficient

2 Introduction

High-performance fighter aircraft with external stores are required to operate with high maneuverability in the transonic flight regime. In this regime, the potential exists for encountering transonic nonlinear flutter, known as limit-cycle oscillation (LCO). LCO is a limited amplitude, self-sustaining oscillation produced by an aerodynamic-structural interaction, which for the cases of interest, is exasperated by the occurrence of shock waves on the surface of the wing and/or stores. LCO results in an undesirable airframe vibration and limits the performance of the flight vehicle.

The main goal of the current work is to gain understanding of the fundamental nature of the phenomena underlying store-induced LCO. This form of LCO typically occurs near linear flutter boundaries in the nonlinear, transonic regime (Mach number ranging between 0.8 and 1.1), suggesting that classical flutter predictions using linear aerodynamic theories can be applied to the identification of lightly damped modes that may nonlinearly participate in LCO. Indeed, using traditional approaches, Denegri [1] had limited success in relating observed

store-induced LCO to "hump'' (or "soft'' crossing) modes found in velocity-damping diagrams. However, in many cases, the linear approach is inadequate in predicting response characteristics of vehicle configurations in the transonic regime.

The transonic regime differs from the linear, subsonic regime by the appearance of shocks. These structures may strongly interact with vehicle boundary layers, with the possible consequences of flow separation or significant shock movement. In a coordinated manner, we examine the ability of aeroelastic models of varying fidelity to predict accurately LCO onset and amplitude. Models based on linear analysis, transonic small-disturbance theory (TSDT), and TSDT with interactive boundary layer are considered. Through this approach, we discern: (1) the limitations of linear theory for LCO prediction vis-à-vis the simplest nonlinear theory capable of producing weak shocks; (2) the ability of TSDT to predict store-induced LCO in inviscid flow, and (3) the effects of viscosity on store-induced LCO.

Two computational methodologies are employed in this investigation: the MSC/NASTRAN aeroelastic analysis program, the TSDT-based NASA/LaRC CAPTSDv computational aeroelasticity algorithm for inviscid and viscous flow.

3 Problem Formulation

The wing studied herein is derived from the "heavy" version of the original Goland wing. Like the original, the heavy wing is structurally represented by a beam, but with additional non-structural mass, as defined by Eastep and Olsen [2]. This latest version, referred to as the Goland$^+$ wing, is a heavy wing modeled with a box structure to enable a variety of store attachment options.

3.1 Geometry

The Goland$^+$ wing is rectangular and cantilevered from the midplane. A planform schematic is given in Fig. 1 (including store). The wing span and chord are 20 and 6 ft. respectively. The airfoil section is constant along the span of the wing and is chosen to be that of a symmetric, parabolic-arc airfoil, defined by $z = 2\ \tau_w\ x\ (1 - x/c_w)\quad (0 \le x \le c_w)$. The wing-tip store is mounted flush to the wing tip (see Fig. 1), with a chord of 10 ft., a span of 1 ft. and a stream wise offset of 3 ft. The sectional shape of the store is also described by a parabolic arc . An additional description of the wing/store configuration is given in [3].

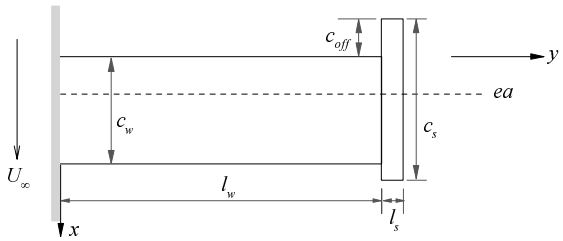

Fig. 1: Goland$^+$ Wing geometry

3.2 Wing Structure and Inertial Properties

The geometry of the wing is simple. The origin is at the mid-height of the root of the leading edge spar. The three spars are un-swept and placed at 0, 2 and 4 ft along the chord. Eleven ribs are evenly spaced on 2 ft centers along the span. Shear elements are placed at the intersections of the spars and ribs, with 10 elements per spar and 2 elements per rib. Next, each spar and rib is 0.33334 ft high and each cell defined by the spars and ribs is capped with a single wing skin membrane element.

The mass properties of this wing are modeled by placing lumped masses with no rotational inertia at each grid point. The lumped masses are sized to match the mass properties (total mass, *cg,* and inertia) of the heavy Goland wing. The details of this model are described in [3].

The final step in developing the built-up model is sizing the elements so that its structural dynamic characteristics match those of the beam model Goland wing. For this model development, the elements are sized to minimize the error between the first three frequencies of the built-up and beam models.

3.3 Store Mass and Linkage

The store configuration examined in this work is that of a tip store. This store structure is

modeled as a series of rigid bar elements that result in a 10 ft long rigid bar. The resultant bar is centered 0.5 ft outboard of the wing tip and 2 ft aft of the wing leading edge. The store is then rigidly connected to the six wing tip grid points.

The mass properties of the tip store match the properties of one two foot section of the wing: a mass of 22.496 slugs and a rotational inertial of 50.3396 slug-ft^2. During this study, the position of the store mass is fixed at the lateral and vertical centers of the store (i.e., y = 20.5 ft and z = 0 ft).

4 Computational Aeroelasticity Methods: CAPTSD and CAPTSDv

CAPTSD solves the three-dimensional, transonic, small-disturbance, potential-flow equations for partial and complete aircraft configurations [4]. A viscous-inviscid interaction version of CAPTSD, known as CAPTSDv, has been developed [5] and applied to a variety of problems involving mildly separated and separation onset flows [6]. The method couples the inviscid CAPTSD algorithm with an inverse integral boundary layer model. In this investigation, a single version of the CAPTSDv algorithm is used to perform both inviscid and viscous aeroelastic analysis .

5 Results

5.1 Physical Conditions

The aeroelastic analysis is carried out with enforced consistency between velocity and dynamic pressure, assuming constant density at sea-level conditions. Mach number is treated as an independent variable, such that match-pointed conditions are not generally achieved. Structural damping is assumed to vanish for all baseline cases investigated.

5.2 Summary of Grid Construction

Three grids are constructed for the CAPTSDv calculations reported in this paper. Owing to the geometry of the wing/store configuration and the mid-plane formulation of the surface boundary condition used in CAPTSDv, these grids are rectilinear. Clustering of grid points is enforced along the edges of the geometry and normal to the wing and store surfaces. The first grid (G1) is used for inviscid, clean-wing and wing/store (store mass only) computations; the second grid (G2) is used for inviscid, wing/store computations, and the third grid (G3) is used for viscous clean-wing and wing/store (store mass only) computations.

A view of grid G2 in the x-y plane in the neighborhood of the wing/store configuration is shown in Fig. 2 to illustrate the effect of grid clustering along the combined planform.

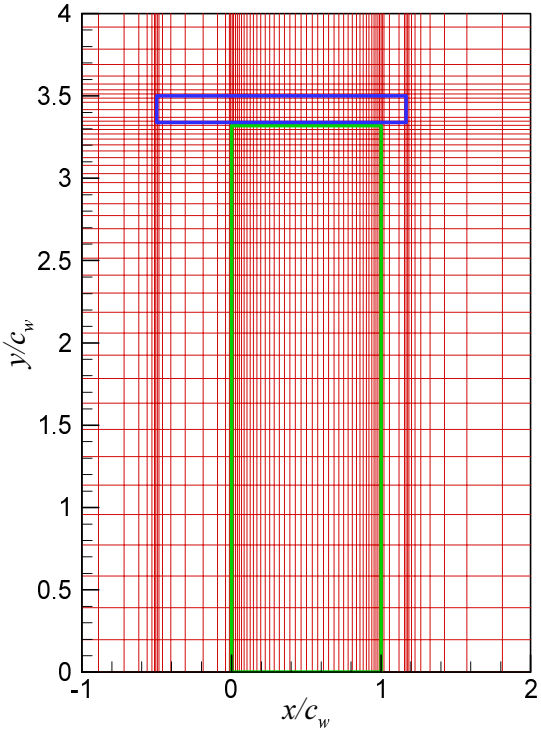

Fig. 2: CAPTSDv computational grid (G2) for the Goland$^+$ Wing. Grid lines (red); wing boundary (green); store boundary (blue).

5.3 Modal Analysis

Modes of the structural model are computed with MSC/NASTRAN and then splined to aerodynamic surface grids (specified at z = 0) with the infinite plate spline, as implemented by Harder and Demaris[7]. The results given in this paper are obtained by retaining the 4 modes of lowest frequency in the aeroelastic analysis and by excluding in-plane modes.

5.4 Linear Analysis

To determine a parameter space (velocity and Mach number for specified altitude) where store-induced LCO possibly exists, a linear flutter analysis of a clear wing and a wing/tip store combination is conducted. The linear flutter speeds (those from linear aerodynamic theories) are determined from data calculated from the *p-k* method of MSC/NASTRAN. The flutter and divergence instabilities can be determined from an inspection of calculated data in graphical form, the so-called *V-g* and *V-ω* diagrams. These diagrams are shown in Fig. 3 (clean wing) and Fig. 4 (wing with tip store mass) for a selected Mach number of 0.92. From Fig. 3, the flutter speed of a clean wing is determined by the first crossing of one of the modes from negative to positive values of the damping parameter, *g* (i.e., 334 ft/sec), and a corresponding flutter frequency of 2.17 HZ. Additionally, shown in Fig. 3 is a divergence instability, whose speed is determined by the simultaneous occurrence of zero damping and zero frequency for another mode (i.e., 630 ft/sec).

The *V-g* diagram of the clean wing is compared to the *V-g* diagram of the wing/store configuration (mass only), shown in Fig. 4, when the store *cg* is located 1.75 ft upstream of the wing elastic axis (equivalent to the store pitch axis). By comparing the two diagrams, it is seen that the flutter speed is increased to 559 ft/sec when the store *cg* is placed at this position and that the severity of the flutter instability of the clean wing has been reduced (reflected by less damping). The flutter mode of the wing/store has been converted into a "hump," or lightly damped mode. It is speculated that the initiation of store-induced LCO is associated, in some way, with hump modes, such that the linear flutter investigation defined a beginning region to search for LCO. Of course, since this hump is determined from linear aerodynamics, the region of LCO must be modified by taking into consideration transonic (nonlinear) aerodynamics. This modification is discussed in the following sections for a determination of store-induced LCO.

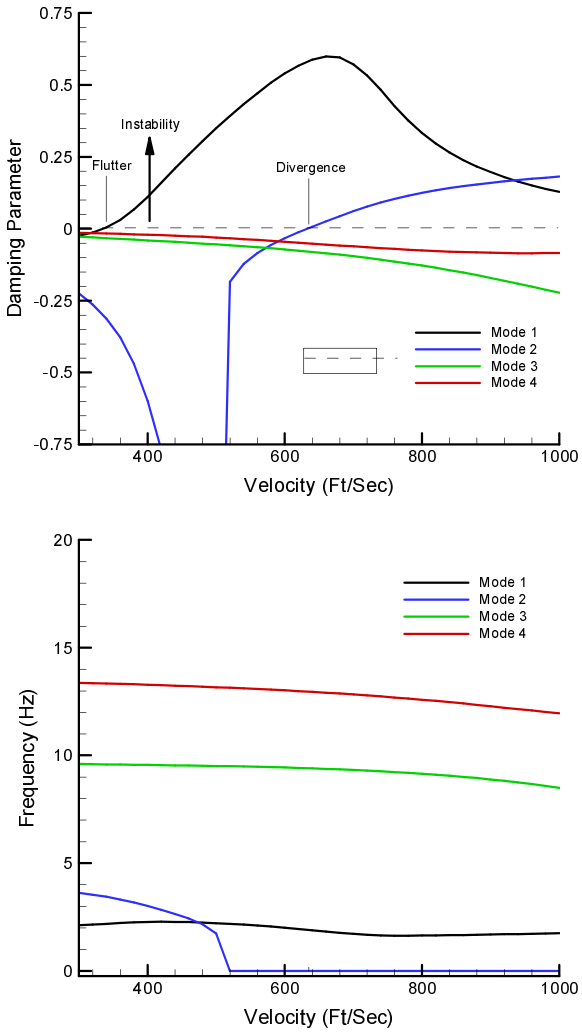

Fig. 3: Flutter characteristics predicted by a linear aeroelastic analysis (MSC/NASTRAN) for the clean Goland+ wing at Mach 0.92.

Linear analysis is carried out for other store mass positions, but not reported herein. These results show the reduction of the peak damping parameter with forward movement of the store mass. The offset position of 1.75 ft (upstream of the wing *ea*) is selected for use in the CAPTSDv calculations reported below, because of the small peak value of *g* attained with this parameter value.

5.5 Flutter Boundaries

Boundaries of flutter and LCO onset are computed for the clean wing configuration and for the wing with store mass (i.e., store not modeled aerodynamically). The flow is assumed inviscid. These results are compared to

those obtained with MSC/NASTRAN using linear analysis. LCO solutions are observed at Mach numbers above Mach 0.9 when the store mass is present; these cases will be discussed in detail in the next section. Flutter and LCO boundaries are compared in Fig. 5. For the clean wing, CAPTSDv predicts a flutter speed of 433 ft/sec at Mach 0.7, a value 3.5% higher than that predicted by MSC/NASTRAN. With the store mass included, CAPTSDv predicts a flutter speed of 648.5 ft/sec (CAPTSDv), a value 6.8% higher than that provided by MSC/NASTRAN. At Mach 0.7, the aerodynamics is linear and the reasonable comparisons between CAPTSDv and MSC/NASTRAN are to be expected. CAPTSDv clearly confirms that forward movement of the store mass has a stabilizing effect on the aeroelastic system for Mach numbers at or below 0.9.

As Mach number increases beyond 0.7, the clean-wing flutter boundary obtained with CAPTSDv develops a transonic dip with a minimum flutter speed (355 ft/sec) at about Mach 0.88. The boundary is much flatter when the store mass is included; flutter speed averages around 645 ft/sec. Both boundaries show a rapid increase in flutter speed near Mach 0.9. However, at selected Mach numbers between 0.90 and 0.95 (0.91, 0.92, 0.93, and 0.94) with the store mass present, LCO solutions are observed. These nonlinear oscillations are computed at flight speeds much lower than the nominal, wing/store flutter speed, and, for some Mach numbers, lower than the clean-wing flutter speed. Thus, the presence of the store destabilizes the system at higher Mach numbers in an adverse manner, i.e., to lower flight speeds.

On the flutter boundary for the wing/store configuration, two different flutter modes are observed. These are contrasted in terms of the computed modal participations for Mach 0.84 and Mach 0.9, as shown in Fig. 6 and Fig. 7. Note that unstable test points are selected above the flutter boundary: U = 750 ft/sec at Mach 0.84 (flutter at 642.5 ft/sec) and U = 850 ft/sec at Mach 0.9 (flutter at about 825 ft/sec). Two different frequencies of divergent oscillation are observed: 1.90 Hz (Mach 0.84) and 9.52 Hz (Mach 0.90). These frequencies are somewhat larger than the natural frequencies corresponding to modes 1 (1.69 Hz) and 3 (9.17 Hz), respectively. For both flutter modes, the phase relationships between peak lift and moment are the same (about 180 degrees out of phase).

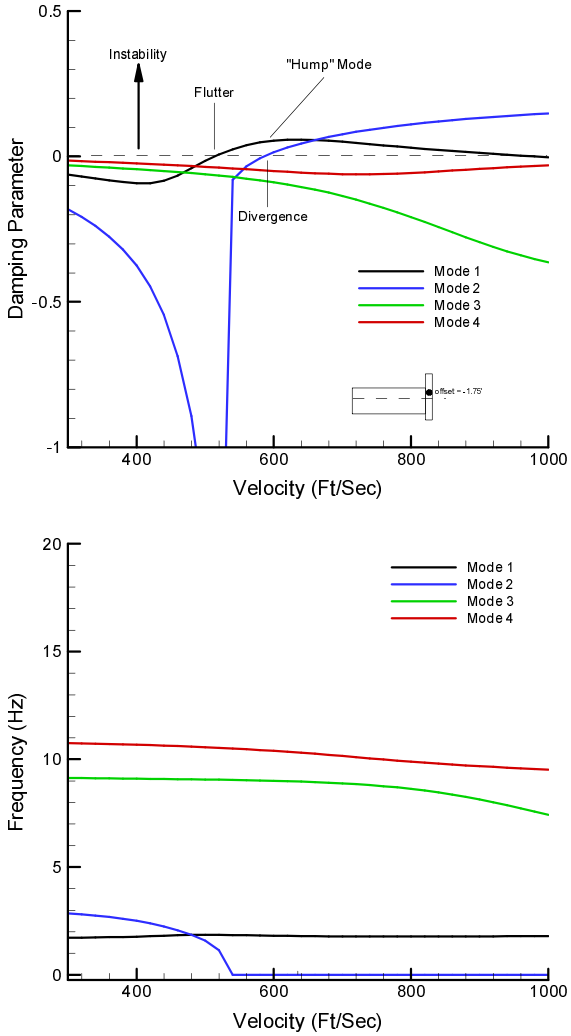

Fig. 4: Flutter characteristics predicted by a linear aeroelastic analysis (MSC/NASTRAN) for the Goland+ wing with tip store mass at Mach 0.92.

A switching of flutter modes is perhaps suggested by the linear MSC/NASTRAN results shown for Mach 0.92 in Fig. 3 and Fig. 4 (the results for Mach 0.9 are not markedly different). The effect of nonlinearity appears to be large in terms of stabilizing the interaction between modes 1 and 2, predicted by MSC/NASTRAN

to occur at about 560 ft/sec. At a larger frequency, coalescence of modes 3 and 4 is evident in the MSC/NASTRAN results at a flight speed of about 800 ft/sec, a velocity near the flutter speed predicted by CAPTSDv.

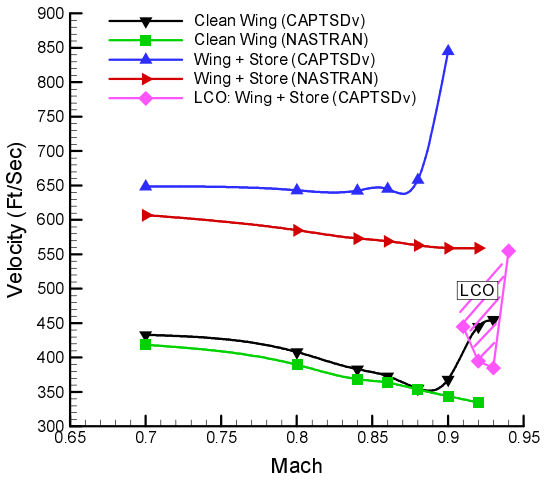

Fig. 5: Comparison of flutter and LCO boundaries computed with inviscid CAPTSDv and MSC/NASTRAN.

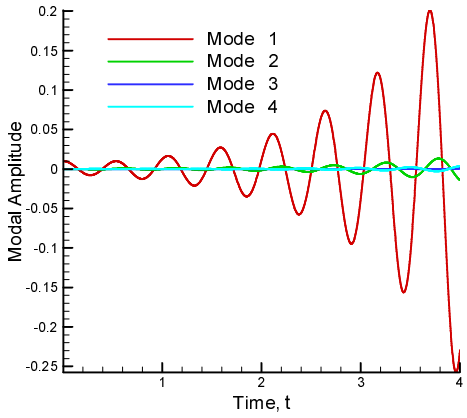

Fig. 6: Modal amplitude histories calculated with inviscid CAPTSDv at Mach 0.84 (U = 750 ft/sec).

5.6 Store-Induced Limit-Cycle Oscillation

In a Mach number range between 0.91 and 0.95, fully developed LCO states are computed with CAPTSDv for the wing/store configuration, excluding store aerodynamics (see Fig. 5). As will be shown later, the effect of including store aerodynamics is not significant, while the effect of viscosity is to reduce LCO amplitude. Two types of LCO are observed: (1) an expected form involving significant time-periodic oscillations of the aeroelastic system that will be described first and referred to as simply LCO, and (2) an unexpected form with very small amplitudes (~3 orders of magnitude less in magnitude) that will be described second and referred to as "embryonic" LCO, or ELCO.

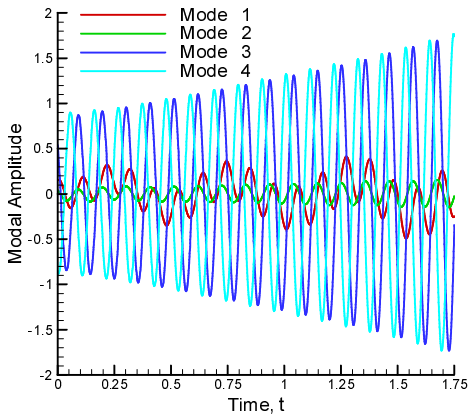

Fig. 7: Modal amplitude histories calculated with inviscid CAPTSDv at Mach 0.90 (U = 850 ft/sec).

As shown in Fig. 5, LCO is observed over a restricted range of Mach numbers. Generally, LCO amplitudes increase with increasing velocity, and for sufficiently large velocities, computed oscillations become so large that the assumptions of TSDT become invalid. Attention is first given to Mach 0.92, where LCO is first observed at U = 390 ft/sec for inviscid flow (onset occurring between 385 and 390 ft/sec) and U = 410 ft/sec for viscous flow (onset occurring between 390 and 410 ft/sec). It should be noted that the onset of LCO is computationally expensive to obtain, since very large integration times are necessary for the aeroelastic system to approach time-asymptotic behavior at values of flight speed near critical. In these calculations, the initial state is defined by a flow solution given by a rigid-body calculation, and the modal amplitudes are assumed to vanish, except for the first mode, which is assigned an initial value of 0.01.

Flutter responses predicted with inviscid CAPTSDv, for the wing with store mass configuration, are shown in Fig. 6 (Mach 0.84)

and Fig. 7 (Mach 0.90) based on modal participation. At Mach 0.84, the response is dominated by mode 1 (first bending), which has a natural frequency of 1.90 Hz. At Mach 0.90, the response is dominated by modes 3 and 4 (torsion modes), which have natural frequencies of 9.17 Hz and 10.8 Hz, respectively. The response frequency is 9.52 Hz.

The slow growth of lift coefficient to its asymptotic value is shown in Fig. 8 for $U = 410$ ft/sec, assuming inviscid flow. LCO frequency is observed to be 2.92 Hz. The computed frequency corresponds to the modal content of the aeroelastic response. As seen in Fig. 9, mode 2 (a natural frequency of 3.05 Hz) dominates the response, with strong participation also from mode 1. At this Mach number and flight speed, the first two modes are much more strongly coupled than in the flutter mode found at low transonic Mach numbers (cf. Mach 0.84), with an associated increase in response frequency.

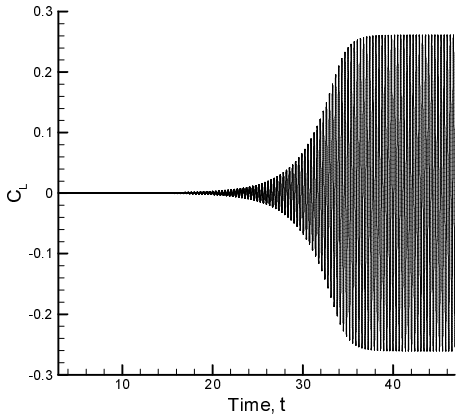

Fig. 8: Lift coefficient time history calculated with inviscid CAPTSDv at Mach 0.92 ($U = 410$ ft/sec).

A similar set of plots of LCO response are shown in Fig. 10 and Fig. 11 for the case of viscous flow, assuming an equivalent flight speed of 410 ft/sec at Mach 0.92. Grid G3 is used for viscous calculations, and the aerodynamics of the store are assumed negligible. LCO amplitude is observed to diminish through the effects of viscosity, and frequency slightly increases to 2.99 Hz. Viscous simulations of LCO are somewhat stiffer than inviscid computations, requiring one Newton sub-iterate per time step for stable calculation.

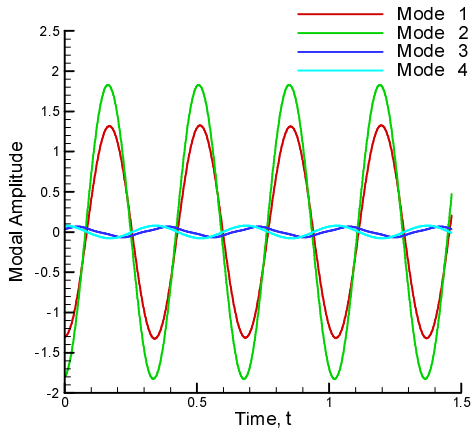

Fig. 9: Modal amplitude histories at LCO calculated with inviscid CAPTSDv wing at Mach 0.92 ($U = 410$ ft/sec).

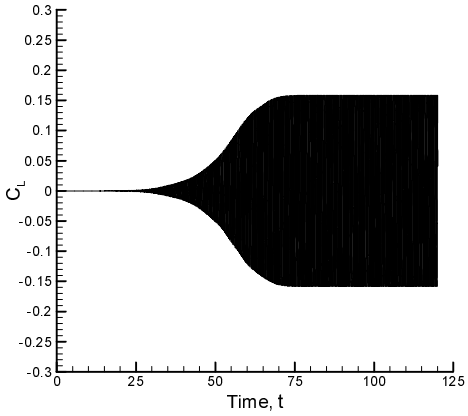

Fig. 10: Lift coefficient time history calculated with viscous CAPTSDv at Mach 0.92 ($U = 410$ ft/sec).

Structural response associated with LCO is contrasted with that of the two flutter modes through visualization of wing-tip motion. The low-speed flutter mode is primarily first bending, which is reflected by a vertical displacement of the wing tip at different times, with introduction of only a slight incidence angle with respect to the free stream. The flutter mode observed at Mach 0.9 is a higher frequency mode involving significant contributions from modes 3 and 4. The response of the wing tip involves both pitch and

plunge, with a motion akin to that of a ship moving into ocean waves (a visual rotation about the mid-chord). In the situation of LCO, the response is composed of first bending and first torsion contributions. A pitching motion dominates the resulting movement of the wing tip, with visual rotation about the tip leading edge.

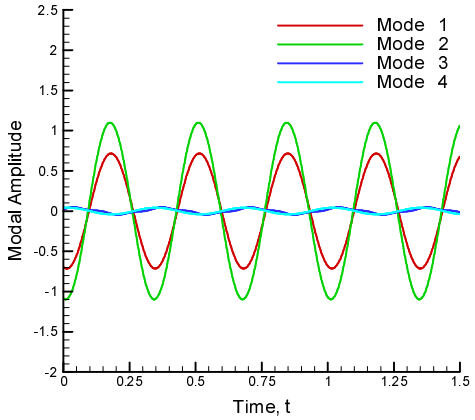

Fig. 11: Modal amplitude histories at LCO calculated with viscous CAPTSDv at Mach 0.92 (U = 410 ft/sec).

LCO solutions of the type described above are not observed at flight speeds below 390 ft/sec for inviscid flow at Mach 0.92. However, at speeds between 340 and 390 ft/sec, sustained oscillations of very small amplitude and less regular character are computed. In this speed range, the magnitude of system oscillations increases very slowly with increasing U. These ELCO states appear to be physical and not numerical in origin, since ELCO formation is found to be persistent to variation of Mach number and various numerical parameters. However, ELCO amplitude is sensitive to structural damping and the numerical precision of the computation. When ζ is increased from the baseline value of 0 to 0.03, ELCO amplitude is reduced by over a factor of 5 at U = 385 ft/sec, and is found to vanish at U = 350 ft/sec. Also, increasing the baseline precision of the computation to double, ELCO amplitude is observed to grow considerably (but remaining at levels small compared to LCO).

A time history of lift coefficient is shown in Fig. 12 for U = 385 ft/sec and assuming baseline values of numerical parameters: the frequency of 2.94 Hz is nearly identical to that found during LCO at U = 410 ft/sec, while peak lift coefficient reaches only about 5×10^{-5}.

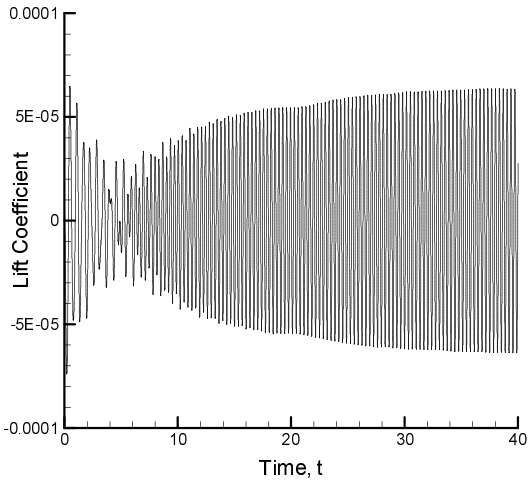

Fig. 12: Low amplitude oscillations at Mach 0.92 (U = 385 ft/sec).

5.7 LCO Sensitivities

The variation of LCO amplitude with respect to changes in flight speed at Mach 0.92 is computed for three categories of analysis: inviscid analysis of wing with store mass (grid G1); inviscid analysis of wing with store modeled aerodynamically (grid G2), and viscous analysis of wing with store mass (grid G3). Results are compared in Fig. 13 to show the effects of varying the level of modeling fidelity within the context of transonic small-disturbance theory. Assuming inviscid flow, it is observed that modeling the store aerodynamically has little impact on the onset or computed amplitude of LCO. However, at speeds exceeding 420 ft/sec, solutions can not be stably computed. In these cases of increased wing-tip twist, numerical destabilization appears to be a result of a very large, localized, pressure spike observed in the region of the juncture between the store and the wing leading edge. This destabilization occurs at about the speed for which LCO amplitude is predicted to grow rapidly when store aerodynamics are ignored; peak lift coefficient begins to take a large jump at U = 427 ft/sec with this approximation. At speeds exceeding this value, the validity of the

computed inviscid solutions is considered to be diminished, owing to the small-disturbance nature of the methodology. As described above for U = 410 ft/sec, the effect of viscosity is to diminish LCO amplitude. When the boundary layer thickness is modeled, no large increase in LCO amplitude is observed, and peak lift coefficient remains bounded by 0.26 over the range of speeds examined, thus reducing the deformation of the wing and extending the speed range over which the assumption of small disturbances is arguably satisfied. Near the bifurcation point, at U = 388 ft/sec, non-unique states are observed. One state, obtained with the baseline initial conditions exhibits very small-amplitude ELCO behavior, while the other state, obtained by restarting the aeroelastic solution from U = 390 ft/sec, exhibits LCO behavior. However, as velocity is reduced below 388 ft/sec, only ELCO is observed, and as velocity is increased above this same speed, only LCO is observed. These inviscid results are indicative of the presence of a subcritical bifurcation just above this speed, causing relatively large jumps in LCO amplitude over a small range of flight speeds. This phenomenon is explored further below for Mach 0.93.

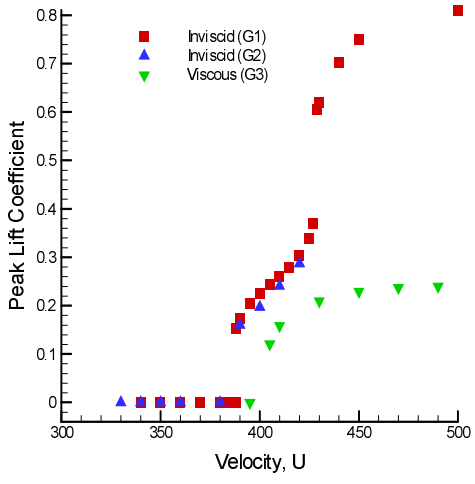

Fig. 13: Comparison of LCO response boundaries for different CAPTSDv analyses at Mach 0.92. G1 – clean wing, inviscid; G2 – tip store aerodynamics, inviscid; G3 – viscous.

As stated above for the results computed at Mach 0.92 (cf. Fig. 13), the onset of LCO is subcritical when inviscid flow is assumed. This is also observed at Mach 0.93, as shown in detail in Fig. 14 (for the baseline condition of vanishing root angle-of-attack). For this comparison, aeroelastic solutions are computed using two kinds of initial conditions: the initial conditions described above, and initialization of the flow field using a fully developed LCO solution obtained at a higher velocity. It is seen that the latter class of initial condition produces fully developed LCO solutions for a small range of velocities (noted at 386 ft/sec and 388 ft/sec) at which the former class of initial condition does not produce LCO. While the range of hysteresis is slight, the subcritical nature of the bifurcation does explain the rather large jumps in amplitude observed beyond the critical points.

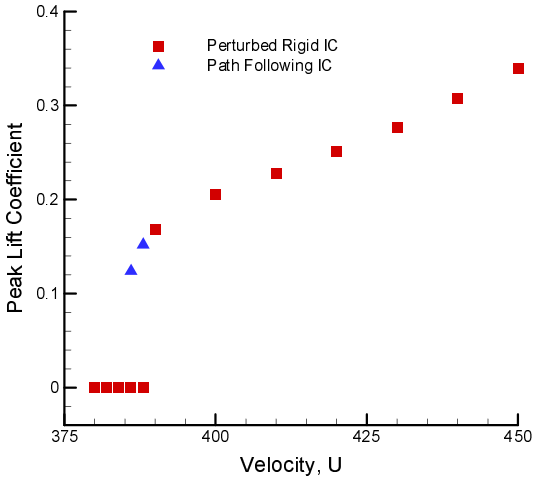

Fig. 14: Demonstration of subcritical Hopf bifurcation and non-unique aeroelastic behavior at Mach 0.93, calculated using two different initial conditions.

Not surprisingly, over the range of Mach numbers that sustain LCO, amplitude of response is found to be highest over the midsection of the range. This is shown in Fig. 15 for a velocity of 410 ft/sec. The response near the low-Mach boundary of the LCO region is characteristic of the subcritical response shown in Fig. 13 and Fig. 14. However, at the high-Mach boundary of the LCO region, the computed results are not suggestive of non-unique flow responses.

6 Summary and Conclusions

A class of limit-cycle oscillations was observed for a rectangular wing with tip store. These LCOs occurred at speeds lower than that predicted using linear aerodynamics and at speeds lower than that computed for the clean-wing configuration. The form of the bifurcation was subcritical, such that LCO amplitude jumped abruptly as Mach number increased beyond a critical value. However, it was also found that as Mach number increased to a critical value (~0.94–0.95), LCO states could no longer be sustained. For the configurations examined, the presence of LCO was insensitive to the inclusion of store aerodynamics in the aeroelastic model. Also, the effect of viscosity was to diminish LCO amplitude. A second class of LCO solutions with small amplitude was observed that occurred over a range of speeds below critical, i.e., prior to the initiation of LCOs characterized by large-amplitude aeroelastic response. These states were found to be sensitive to structural damping, such that addition of nominal levels of damping was sufficient to overcome the phenomenon.

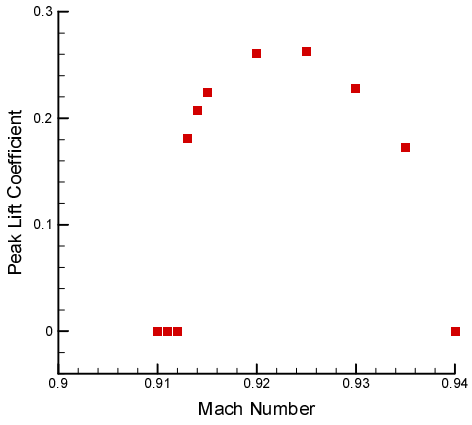

Fig. 15: Variation of LCO response of the clean wing for different Mach numbers at U = 410 ft/sec.

The search for LCO states was conducted in two steps. First, linear theory was employed in the identification of "hump" modes, which corresponded to placement of the store mass near the wing leading edge. Such characteristic aeroelastic responses were expected to point to conditions susceptible to LCO. Second, LCO states were computed using the transonic small-disturbance theory algorithm CAPTSDv, assuming both inviscid and viscous flow. This nonlinear mathematical formulation was sufficient to capture properly weak shock formation and movement.

Acknowledgements

The first author received funding support for this research from the National Research Council Senior Research Associateship Program. Additionally, this work was sponsored by the Air Force Office of Scientific Research.

References

[1] Denegri, C. M., "Limit Cycle Oscillation Flight Test Results of a Fighter with External Stores," Journal of Aircraft, Volume 37, Number 5, September-October 2000, pp. 761-769.

[2] Eastep, F. E., "Transonic Flutter Analysis of a Rectangular Wing with Conventional Airfoil Sections," AIAA Journal, Volume 18, Number 10, October 1980, pp. 1159-1164.

[3] Beran, P. S.,Khot, N. S.,Eastep,F. E., Snyder,R. D., Zweber, J. V., Huttsell, L. J. and Scott, J. N. ,"The Dependence of Store-Induced Limit-Cycle Oscillation Predictions on Modeling Fidelity." Presented at the RTO Applied Vehicle Technology Panel Symposium on "Reduction of Military Vehicle Acquisition Time and Cost Through Advanced Modeling and Virtual Product Simulation," Paris France, 22-25 April,2002, Paper # 44.

[4] Batina, J. T., "Unsteady Transonic Algorithm Improvements for Realistic Aircraft Applications," *Journal of Aircraft*, Volume 26, February 1989, pp. 131-139.

[5] Howlett, J. T., "Efficient Self-Consistent Viscous Inviscid Solution for Unsteady Transonic Flow," *Journal of Aircraft*, Volume 24, November 1987, pp. 737-744.

[6] Edwards, J. W., "Calculated Viscous and Scale Effects on Transonic Aeroelasticity," AGARD-R-822, Numerical Unsteady Aerodynamic and Aeroelastic Simulation, March 1998, pp. 1-1 – 1-11.

[7] Harder, R. L. and Desmaris, R. N. " Interpolation Using Surface Splines," Journal of Aircraft, Vol.9, No2, 1972.